The effect of rapid relative humidity changes on fast filter-based aerosol particle light absorption measurements: uncertainties and correction schemes

Sebastian Düsing[1], Birgit Wehner[1], Thomas Müller[1], Almond Stöcker[2], Alfred Wiedensohler[1]

[1]Leibniz Institute for Tropospheric Research (TROPOS), 04318 Leipzig, Germany
[2]Ludwig-Maximilians-University Munich, Department of Statistics, 80539 Munich, Germany

Correspondence to: Sebastian Düsing (duesing@tropos.de)

Abstract.

Measuring vertical profiles of the particle light absorption coefficient by using absorption photometers may face the challenge of fast changes in relative humidity. These absorption photometers determine the particle light absorption coefficient due to a change in light attenuation through a particle-loaded filter. The filter material, however, takes up or releases water with changing relative humidity (*rh* in %), influencing thus the light attenuation.

A sophisticated set of laboratory experiments was therefore conducted to investigate the effect of fast *rh* changes (d*rh*/d*t*) on the particle light absorption coefficient (σ_{abs} in Mm^{-1}) derived with two absorption photometers. The *rh* dependency was examined based on different filter types and filter loadings with respect to loading material and loading areal density. The Single Channel Tri-Color Absorption Photometer relies on quartz-fiber filter and the microAeth® MA200 is based on a Polytetrafluoroethylene (PTFE) filter band. Furthermore, three cases were investigated: clean filter, filter loaded with black carbon (BC) and filter loaded with ammonium sulfate. The filter loading areal densities (ρ^*) ranged from 3.1 to 99.6 mg m^{-2} in the case of the STAP and ammonium sulfate, 1.2 to 37.6 mg m^{-2} considering the MA200. Investigating BC loaded cases, ρ^*_{BC} was in the range of 2.9 to 43.0 and 1.1 to 16.3 mg m^{-2} for the STAP and MA200, respectively. In addition, the effect of a silica-bead based diffusion on the *rh* effect was investigated.

Both instruments revealed opposing responses to relative humidity changes (Δrh) with different magnitudes. The STAP shows a linear dependence to relative humidity changes. The MA200 is characterized by a distinct exponential recovery after its filter was exposed to relative humidity changes. At a wavelength of 624 nm and for the default 60-second running average output, the STAP reveals an absolute change in σ_{abs} per absolute change of *rh* ($\Delta\sigma_{abs}/\Delta rh$) of 0.14 Mm^{-1} $\%^{-1}$ in the clean case, 0.29 Mm^{-1} $\%^{-1}$ in the case of BC loaded filters, and 0.21 Mm^{-1} $\%^{-1}$ considering filters loaded with ammonium sulfate. The 60-second running average of the particle light absorption coefficient at 625 nm measured with the MA200 revealed a response of around -0.4 Mm^{-1} $\%^{-1}$ for all three cases. Whereas the response of the STAP varies over the different loading materials, in contrast the MA200 was quite stable. The response was for the STAP in the range of 0.17 Mm^{-1} $\%^{-1}$ to 0.24 Mm^{-1} $\%^{-1}$ considering ammonium sulfate loading and, in the BC loaded case 0.17 Mm^{-1} $\%^{-1}$ to 0.62 Mm^{-1} $\%^{-1}$, respectively.

In the ammonium sulfate case, the minimum response shown by the MA200 was -0.42 Mm^{-1} $\%^{-1}$ and -0.36 Mm^{-1} $\%^{-1}$ at maximum, -0.42 Mm^{-1} $\%^{-1}$ and -0.37 Mm^{-1} $\%^{-1}$ in case of BC loading, respectively. Using the aerosol dryer upstream, the STAP did not change the behavior, but the amplitude of the observed effect was reduced by a factor of up to three.

A linear correction function for the STAP was developed here. It is provided by correlating 1 Hz resolved recalculated particle light absorption coefficients and *rh* change rates. The linear response is estimated with 10.08 Mm^{-1} s^{-1} $\%^{-1}$. A correction approach for the MA200 is also provided, however, the behavior of the MA200 is more complex. Further research and multi-instrument measurements have to be conducted to fully understand the underlying processes, since the correction approach resulted in different correction parameters across various experiments. However, the exponential recovery after the filter of the MA200 experienced a *rh* change could be reproduced. Though, the given correction approach has to be estimated with other *rh* sensors as well since each sensor has a different response time. And, for the given correction approaches the uncertainties could not be estimated mainly due to the response time of the *rh* sensor. Therefore, we do not recommend to use the given approaches. But, they showing in the right direction and besides the imperfections they are useful to at least estimate the measurement uncertainties due to relative humidity changes.

Due to our findings, we recommend to use an aerosol dryer upstream of absorption photometers to reduce the *rh* effect significantly. Furthermore, when absorption photometers are used in vertical measurements, the ascending or descending speed through layers of large *rh* gradients has to be low to minimize the observed *rh* effect. But this is simply not possible in some scenarios especially in unmixed layers or clouds. Additionally, recording the *rh* of the sample stream allows correcting for the bias during post processing of the data. This data correction leads to reasonable results, according the given example in this study.

1 Introduction

Black carbon (BC) and its light-absorbing properties has significant influence on the Earth's climate, and its contribution is associated with major uncertainties, in particular due to its vertical distribution (Zarzycki and Bond, 2010). In addition, it is suspected to affect human health (WHO, 2012). Absorption photometer are feasible instruments to measure the light absorbing properties of aerosol particles. These photometers measure the aerosol particle light absorption coefficient (σ_{abs}) by detecting the change of attenuation of light due to deposited aerosol particle mass on sample filter. They have been installed on airship platforms (Rosati et al., 2016), tethered balloon platforms (Ran et al., 2016; Ferrero et al., 2014, Ferrero et al., 2016) or unmanned aircraft systems (UAS; Markowitz et al., 2017, Telg et al., 2017, Bärfuss et al., 2018) to address the vertical BC distribution. To investigate human exposure to health-harming BC-containing aerosol particles from combustion sources, they have been used for mobile measurements (Capeda et al., 2017 and references therein; Alas et al, 2018).

Subramanian et al. (2007), Vecchi et al. (2013) and Lack et al. (2008) have shown, that liquid-like brown carbon can significantly bias filter-based absorption measurements since this organic carbon wraps around filter fibers and alters their structural properties. Aerosol samples contain water vapor represented by its relative humidity (*rh*). Similar to liquid-like

brown carbons, water vapor can be adsorbed through the filter material or bound to the binding material within the filter during the sampling process. A variety of filter materials is used in absorption photometers and the water uptake is different across various materials. Hence, changes in the aerosol *rh* can affect the aerosol particle light absorption measurements differently. Nessler et al. (2006) has shown to which extent sudden changes in relative humidity (*rh*) can influence measurements of a Particle/Soot Absorption Photometer (PSAP; Radiance Research, Seattle, WA) and an Aethalometer for clean filter material and loaded with BC, whereas Cai et al. (2014) has shown the effect for the microAeth® AE51, however, they did not quantify it. However, hygroscopic aerosol particle species such as ammonium sulfate can take up water depending on the relative humidity. The *rh* effect for filters loaded with such aerosol species was never quantified. Furthermore, not all filter materials have been covered within these studies. Summarizing, both, filter material and loading material, may influence the light attenuation of the filter.

The *rh* effect might not be relevant for averaging periods longer than 5 minutes as usually done at stationary measurements on ground (e.g. to address human exposure to BC containing aerosol particles). However, to address vertical profiling of BC with fast *rh* changes, particle light absorption measurements require a high temporal resolution of about seconds.

Telg et al. (2017) presented a study using an unmanned aircraft system (UAS) for vertical profiling of aerosol physical properties including the aerosol particle light absorption coefficient measured by an absorption photometer. In their study, a significant decrease of σ_{abs} at around 1000 m altitude is visible. Considering the other simultaneously measured microphysical aerosol parameters, this decrease is not to be expected. In the WMO/GAW report 227 (2016), it is recommended to conduct aerosol sampling below 40% relative humidity to prevent measurements artefacts due to high relative humidity. Although the measurements of Telg et al. (2017) have been conducted following these recommendations, this is a published example for the bias in σ_{abs} measurements due to fast *rh* changes even for a *rh* below the 40% threshold.

In our study, the *rh* effect is investigated for the small-sized photometers STAP, using a quartz-fiber glass filter, and MA200®, which relies on a Polytetrafluoroethylene (PTFE) filter. We show results of a set of laboratory experiments and address the effect of sudden changes in relative humidity for both absorption photometers. Herein, we consider three different scenarios: a) clean filters, different filter loading densities of b) hydrophobic BC, and c) hydrophilic ammonium sulfate ($(NH_4)_2SO_4$). In all of these cases we also investigated the impact of a silica-bead based diffusion drier to the *rh* effect.

Following scientific questions will be addressed: To which extent do STAP and MA200 are sensitive to *rh* changes, and does different loading with respect to material and areal density contribute to this effect? Can the observed effect be corrected, and which recommendations can be given for the usage of such absorption photometer? This is important because recent developments indicate that lightweight absorption measuring instruments will be used more frequently for airborne applications in the near future.

2 Experiment

2.1 Theory of absorption measurements

Filter-based absorption photometer measuring the decrease of intensity of light which passes through the filter-medium with a specific optical thickness. The decrease of intensity can be described quantitatively according the law of Beer-Lambert:

$$\ln(I) = \ln(I_0) + \sigma_{\mathrm{ATN}}(\lambda) l, \tag{1}$$

where I is the attenuated intensity of light with a wavelength λ with a raw intensity I_0, attenuated along a path l through a medium with an light attenuation coefficient σ_{ATN}. The path length l can also be interpreted as the length of a column of aerosol passing through the sample area of the filter spot A_i of the instrument (subscript i), whereas the particles are collected and accumulated in the filter. But, a reinterpretation of the path length does not mean that the result is the particle light absorption coefficient, but still the light attenuation coefficient. The path length l can be calculated by the volume, which flows at a certain rate (volume flow rate; Q_i), for a time Δt through the sample area A_i. Based on Eq. (1), this results into:

$$\ln(I(t)) = \ln(I(t - \Delta t)) + \sigma_{\mathrm{ATN,i}}(\lambda) \frac{Q_\mathrm{i} \Delta t}{A_\mathrm{i}} \tag{2}$$

While aerosol particles deposit on the filter the incoming light gets additionally scattered by those particles. Hence the effective pathway of the light through the filter increases due to the multiple scattering. To account for this, Eq. (2) needs *f(τ)*, a transmission (τ) dependent filter-loading correction factor, with:

$$\tau = \frac{I(t)}{I_0}, \tag{3}$$

where I_0 is the light intensity measured for a white, clean filter. For instance, Ogren (2010) reported an updated loading correction function for the PSAP introduced and updated by Bond et al. (1999) defined as:

$$f(\tau) = (1.0796\tau + 0.71)^{-1}, \tag{4}$$

which is also used for the STAP.

Rearranging and applying the filter loading correction to the attenuation coefficient Eq. (2) will give the particle light absorption coefficient:

$$\sigma_{\mathrm{abs,i}}(\lambda) = \ln\left(\frac{I(t)}{I(t-\Delta t)}\right) \frac{f(\tau) A_\mathrm{i}}{Q_i \Delta t} \tag{5}$$

Water has a refractive index of 1.33+i1.5e-9 at 532 nm wavelength. Hence it interacts with incoming electromagnetic radiation. If the filter is exposed to relative humidity changes the light attenuation of the filter changes, since the water binds to the filter itself (Caroll, 1976 and Caroll, 1986). Since a variety of filter materials, with different physical properties exist, we suspect that magnitude and sign of the light attenuation coefficient can vary with the filter material. The hypothesis is that the change rate of the *rh* (d*rh*/d*t*) directly determines the magnitude of the particle light absorption coefficient, which depends on the difference of two subsequent attenuation measurements.

The effect of changes in the relative humidity on particle light absorption measurements contains of two parts. First, the interaction of the filter with the *rh* by its own. Second, hygroscopic particles change their optical properties by the water uptake and loss due to growing and shrinking. Hence, aerosol particles under varying relative conditions will also have an effect on the reported particle light absorption coefficient.

Some absorption photometer such as the STAP directly report measurements of the aerosol particle light absorption coefficient σ_{abs}, some, for instance the MA200, report measurements of the equivalent black carbon (eBC; Petzold et al. (2013)) mass concentration (M_{eBC}). eBC mass concentrations can be converted to σ_{abs} with:

$$\sigma_{\mathrm{abs}} = M_{\mathrm{eBC}} \cdot MAC, \tag{6}$$

in which *MAC* is the mass absorption cross section in $m^2\ g^{-1}$.

Lab-comparison of the eBC mass concentration between a MAAP (Multi Angle Absorption Photometer; Thermo Fisher Scientific, 27 Forge Parkway, 02038 Franklin, MA, USA; Petzold and Schönlinner, 2004) at 637 nm wavelength and MA200 at 625 nm and STAP at 624 nm beforehand the experiment revealed a good agreement within 3% and within 6%, respectively. For the STAP a *MAC* of 6.6 $m^2\ g^{-1}$ was assumed. Since a *MAC* of 6.6 $m^2\ g^{-1}$ is used for the MAAP at 637 nm, in this study we used the σ_{abs} directly provided by the STAP and derived with the mentioned *MAC* in the case for the MA200, which already accounts for multiple scattering and filter loading corrections.

2.2 Instrument description

As mentioned before, we investigated two filter-based absorption photometers, which are described in the upcoming sections. The Single Channel Tri-Color Absorption Photometer (STAP; Brechtel Manufacturing Inc, 1789 Addison Way, Hayward, CA 94544, USA) and the MA200 (AethLabs, 1640 Valencia St, Suite 2C, San Francisco, CA 94110, USA) use different filter materials. The STAP relies on a quartz-fiber glass filter, whereas the MA200 is based on a Polytetrafluoroethylene (PTFE) filter. Since their behavior under fast changes of the relative humidity is not described yet and we investigate both instruments in this study.

2.2.1 Single Channel Tri-color Absorption Photometer (STAP)

The Single Channel Tri-color Absorption Photometer. This photometer detects light intensities behind two quartz-fiber glass filter (PALL LifeScience, Pallflex Membrane Filters Type E70-2075W) at three wavelengths (450, 525 and 624 nm). On the first filter, the sample filter, the light attenuates due to deposited particulate matter. The second filter, the reference filter, is located downstream the sample filter and allows blank filter reference light intensity measurements.

By default, the particle light absorption coefficient is determined internally using 60 s averages of the raw intensity measurements for both filter spots. Therefore, in Eq. (5) *I(t)* is defined as:

$$I(t) = \frac{I_{\mathrm{smp},\lambda}}{I_{\mathrm{ref},\lambda}}, \tag{7}$$

where I_{smp} and I_{ref} is the intensity of light at the certain wavelength λ behind the sample (smp) and blank reference (ref) filter, respectively. Nevertheless, all raw measurements are recorded with a time resolution of 1 Hz allowing a recalculation of σ_{abs} at this time resolution. The volumetric flow is set to one liter per minute (lpm). According to the manual, at an internal averaging interval of 60 s, the measurement uncertainty is specified to 0.2 Mm^{-1}. The spot diameter is ~4.8 mm which leads to a sample area of A_{spot} ~1.75e-5 m^2.

2.2.2 MA200

The second instrument used here is the microAeth® MA200 is a small sized (13.7 x 8.5 x 3.6 cm; 420g), absorption photometer measuring the attenuation of light at 5 wavelengths (375, 470, 528, 625, and 880 nm; 625 nm are investigated in this study) due to deposited particulate matter on a PTFE filter band.

Similar to the STAP, the MA200 detects light intensities behind a sample and reference spot. The particulate matter samples on a sample spot with 3 mm diameter leading to a sample area of A_{spot} ~0.71e-5 m^2. The reference spot of same area allows for blank filter measurements. M_{eBC} is determined under the assumption that the change of attenuation is proportional to the deposited eBC mass. The measurements were recorded with a 1 Hz time resolution. With the DualSpot® technology the instrument is able to reduce uncertainties related to loading effects up to 60 % (Holder et al., 2018) but was not functioning at the time of the experiment.

Holder et al. (2018) reported that the measurements are slightly depending on *rh* and *T* of the aerosol sample. However, they observed concentrations of up to 7 mg m^{-3}, at which the observed dependence on humidity and temperature did not influence the measured values significantly. Furthermore, they used another version of the instrument (MA350), which may react differently to changes in humidity and temperature.

2.3 Experimental Setup

The experimental setup is designed to examine the instrument filters in different states. Unloaded filters and differently loaded with black carbon and ammonium sulfate were investigated. The extent to which fast changes in the relative humidity of the air passing through the filter affect absorption measurements was investigated for these conditions.

A miniCAST burner (model 5200, Jing Ltd.) was used to generate soot (black carbon; BC) aerosol particles due to combustion of propane. The produced BC particles stream can be diluted according the needs of the customer. A detailed description of the miniCAST is supplied by (Jing, 1999). Additionally, a solution of ammonium sulfate ($(NH_4)_2SO_4$; solution concentration of 0.05g/ 80 ml) was nebulized to an aerosol and was dried afterwards. Either the ammonium sulfate or the BC aerosol was fed into a 0.5 m^3 stainless steel mixing chamber. A fan within the chamber ensures a well-mixed aerosol.

The scheme of the experimental set up is described in Figure 1. First, two particle free, dry (RH = 0%) air flows were produced. One of the flows was humidified by passing through two glass tubes containing distilled water at room temperature with an inlet and outlet for compressed particle free air. A maximum relative humidity of ~96% was reached. Both, the dry and humidified air flows were mixed together with a Swagelok brass T-shaped flow splitter and it was ensured that the sum of

both mass-flows exceeded 1 lpm (controlled by a mass flow controller). Different *rh* were produced according to the ratios of the dry and humidified air. For this, valves with markings indicating the opening state of the valves were used to reproduce consistent mixing *rh*. The *rh* and *T* of the airflow sampled with the photometer were detected with a temperature and relative humidity sensor (model HYT939, B+B Thermo-Technik GmbH, 78166 Donaueschingen, Germany) within an accuracy of ±1.8% (between 0 and 90% RH) and ±0.2°C (between 0 and 60°C). Furthermore, this sensor has a response time t_{63} of <10s. Additionally, this setup could be used with or without a silica bead-based dryer beforehand the photometers to examine to which extent a dryer dampens the effect of relative humidity changes on the photometer absorption measurements.

Two main setups were used to investigate the effect of changes in real humidity. In the first, the filters of the devices were unloaded and the instruments collected a particle free airflow with adjustable relative humidity to examine the pure filter effect. In the second, the filters of the devices are loaded to a certain degree and afterwards they sample particle-free humidified air which accounts for the combination of both effects, the pure filter effect and the effect induced by the hygroscopic behavior of the particles.

The loading aerosol was split into two streams from one of which the absorption photometer were sampling simultaneously. The other one was sampled with a mobility particle sizer spectrometer (MPSS; working principle explained in e.g. Wiedensohler et al. (2012)) to measure the aerosol particle number size distribution from which the loading mass was estimated. An example of a generated ammonium sulfate aerosol is shown in Figure 2. Furthermore, to examine the loading mass concentration of the generated eBC (soot), the generated BC aerosol was measured also with a MAAP.

3 Results

This chapter will give an overview of the measurement results. The overall behavior of both instruments will be shown for wavelengths of 624 nm in the case of the STAP and 625 nm in the case of the MA200, respectively. A closer look at the behavior of both devices at 1 Hz time resolution shows that both devices differ greatly in quality (see Figure 3). The STAP (red dots and the smooth fit shown as black line) reacts very fast to relative humidity changes (d*rh*/d*t* as purple line) and then returns relatively fast to the zero line. The MA200, on the other hand, also shows a fast response to relative humidity changes, but then shows a distinct exponential recovery (see Figure 3, blue dots and smooth fit shown as orange line) and reports absorption coefficients different from zero although there is no *rh* change.

Therefore, we use an averaging on a 60 second basis to describe the qualitative behavior of both devices. In the case of the STAP, the internal 60 second averaging is used. For the MA200, on the other hand, a 60-second "running average" is applied to the 1 Hz measurements.

The qualitative behavior of both devices is shown as follows. To each absolute change in the relative humidity (Δrh) the corresponding maximum of the excursion of the averaged absorption coefficient ($\Delta\sigma_{abs}$) has been assigned. Where the absolute change of the relative humidity is the difference between the relative humidity at the time of the largest excursion in

the absorption coefficient and the relative humidity at the start of the excursion. This approach also excludes the response time of the *rh* sensor.

First, the results for the pure filter effect will be shown. Afterwards, we present the results of the combined behavior of filter and aerosol particles on the filters. For loaded filters, the combined effect will be shown separated into BC and ammonium sulfate loading.

3.1 Clean filters

In Figure 4, the time series of the measured *rh* upstream the two photometers (upper panel) and of σ_{abs} measured by the STAP (624 nm) and MA200 (625 nm) in the lower panel are shown. The air sampled by the photometers was entirely particle-free. Relative humidity was changed in this time series between 3.1 and 87.7 %. The change rate of *rh* (d*rh*/d*t*) was in the range of around -3.0 to 2.9 % s^{-1}. Whereas the measurements of the STAP ranging between -9.8 and 9.5 Mm^{-1} the running 60 s mean of the MA200 readouts were ranging from to 32.2 to -33.6 Mm^{-1}, respectively. Furthermore, Figure 4 shows the opposing behavior of both instruments. Whereas the STAP reacts to positive change rates of the *rh* with positive particle light absorption coefficients, the MA200 measures negative particle light absorption coefficient and vice versa. Summarizing, this indicates that the different filter materials react opposing to each other.

Subramanian et al. (2008) observed that organic matter produced during low-temperature biomass burning has a liquid, bead-shaped appearance when collected on fibrous filter. Also, these organics can appear as translucent coatings on the filter fibers and therefore change significantly the interaction with incident light. Accordingly, for this study this means that the water in the collection stream can wrap itself around the filter fibers, analogous to the organic materials. Lack et al. (2008) has estimated the bias on filter-based absorption measurement due to loading with organic material. Under conditions with low mass concentrations of organic matter the agreement with photoacoustic-based aerosol light absorption measurements was 12 %. Whereas under conditions where the mass concentration of organic material was 15 to 20 times larger than that of light absorbing carbon, the difference was 50 – 80 %. Therefore, the effect of coating with liquid matter around the fibers is not negligible. In the case of the STAP, the water beads and coating can lead to a higher net reflectance of the filter, which appears darker for the photodiode behind the filter. The instrument interprets this as an increased attenuation and hence as an increased absorption. In addition, the backing material consists of hydrophilic cellulose, which may absorb water under increased relative humidity and thus change its optical properties (Ogren et al., 2017). Compared to the fibrous structure of the quartz-fiber filter, the PTFE filter of the MA200 is a porous, hydrophobic filter. We speculate that these properties result more into a collection of a thin film of water, which could act as an index matching between the refractive indices of the PTFE and air. An additional film with intermediate refractive index reduces the reflectance and thus increases the transmittance leading to a decreased attenuation. Hence, the instrument interprets decreases of the attenuation as negative absorption.

Since the filter in the STAP reveal positive and the filter in the MA200 a negative correlation to relative humidity changes a combination of both filters within one instrument could account for the observed effect. A new developed instrument could use these two different filter materials on two sampling spots to cancel out the effect of each other. Though, more

investigations have to be done, especially to understand the different recovery behaviors and effect magnitudes of the PTFE and quartz-fiber filter.

The overall behavior of both instruments in the case of clean filters is shown in Figure 5 (upper left panel). For all investigated Δrh, the response behavior of the MA200 (R^2 = 0.99) is more stable than the STAP (R^2 = 0.78). However, the response is stronger than the average response of the STAP at the presented wavelength. Whereas the STAP shows a dependency of 0.14 Mm^{-1} $\%^{-1}$, which means an increase in absorption with increasing *rh*, the MA200, shows an opposing behavior with a larger absolute value in the slope of -0.41 Mm^{-1} $\%^{-1}$ (Appendixtable 1). As shown in Fig. 4, for each device the magnitude of the deviation due to positive or negative changes in humidity is approximately the same.

3.2 Loaded filters

Different aerosol types deposit on the filter within the instruments while measuring σ_{abs}. These aerosol types are either hydrophilic or hydrophobic and hence experience water uptake or not under conditions of elevated *rh*. Hereby, the more particle material is deposited on the filter the more water deposits on the filter. Therefore, this section will show the influence of different filter loading materials on the *rh* effect and will also point out the effect of different filter loading mass. The observed effect will include both, the effect for clean filters (the pure filter effect) and the effect of the hygroscopic behavior of the particles loaded onto the filter. But, investigating the effect of the loading material alone is simply not possible since no filter material exist, which is not affected by *rh* changes. Therefore, the presented results are always a combination of the filter effect and the material effect. For both considered loading materials, the mass loaded onto the filters was calculated by multiplying the prevalent loading mass concentration within the mixing chamber with the volume flow rate of the instrument and the loading duration. The filter were loaded to a certain extent with different materials and afterwards the absorption photometer were sampling particle free air with adjustable humidity. The different sample spot areas of the absorption photometers will be considered herein by normalizing the loaded mass with the respective sample spot area. Ongoing this will be referred as filter loading areal density ρ*.

3.2.1 Black carbon

During the experiment the eBC loading mass concentration was estimated with different methods depending on the stability of the mass concentration and loading duration and was ranging between 27.6 and 52.6 µg m^{-3}. In Table 1 ρ^* of eBC per spot area (ρ^*_{eBC}) of both instruments is shown. During experiment #1 (see Table 1) the mean absorption coefficient of the STAP was divided by a *MAC* of 6.6 m^2 g^{-1} since the absorption was stable during the loading period and it's a direct measure from the sampling instrument. For the experiment #2 the loading mass concentration was taken from the average of two consecutive MAAP measurements since the loading period was shorter than 2 minutes which is shorter than the internal averaging period of the STAP so that no stable absorption coefficient readouts could be provided by the STAP. During experiment #3 no MAAP was available and the absorption coefficient measured by the STAP was unstable. We therefore decided to estimate the loaded eBC mass by integrating the absorption coefficient during the loading period and dividing it by

the *MAC*. Four different ρ^*_{eBC} were considered in the case of the STAP, three for the MA200, respectively. Due to the smaller volume flow rate of the MA200, ρ^*_{eBC} is in each corresponding case smaller than ρ^*_{eBC} for the STAP and therefore, if any effects of different loadings are observed these might be not as distinct as for the STAP.

For all considered BC loading cases the averaged response of STAP and MA200 to relative humidity changes is shown in Figure 5 (upper right panel) and corresponding linear fitting and correlation parameters are given in Appendixtable 1. The STAP shows a dependency of 0.29 Mm^{-1} $\%^{-1}$ in this case. This means absolute changes in *rh* affecting the BC loaded filter leading to stronger σ_{abs} deviations than in the clean case. For the MA200, the response of the instrument to rapid changes in *rh* does not depend on the loading material the filter with BC since the regression slope is the same as in the clean case. However, the y-intersects deviate from each other but within 0.6 Mm^{-1}. We assume that this could be due to the lower absolute loading on the filter (15% of the STAP loading because of 0.15 lpm flow rate compared to 1 lpm of the STAP) or the MA200 response is in general independent of the filter loading material.

Considering different loading areal densities, the MA200 shows more or less the same behavior (see Appendixtable 1 and Figure 7).The slope of the linear correlation fit ranges from -0.42 Mm^{-1} $\%^{-1}$ to -0.37 Mm^{-1} $\%^{-1}$ for corresponding loading areal densities of 1.1 to 16.3 mg m^{-2}. The STAP shows a larger variability (Figure 7, left panel, black and gray colors). For ρ^* of 2.8 to 42.9 mg m^{-2} the STAP response ranges from 0.17 Mm^{-1} $\%^{-1}$ to 0.62 Mm^{-1} $\%^{-1}$. However, these results may not be entirely representative since R^2 is only for a loading density of 13.7 mg m^{-2} larger than 0.9 (0.94). Maybe the smaller amount of data points in the other cases explains this. However, the number of data points observed with the MA200 was also small but R^2 is in each case larger than 0.9. Similar to the clean case, for both instruments, drying and humidifying the sample stream to the same extent resulted in a deviation of σ_{abs} with the similar magnitude.

3.2.2 Ammonia sulfate

The loading mass concentration of the $(NH_4)_2SO_4$ aerosol depositing on the filters was estimated by integrating the mean ammonium sulfate aerosol particle volume size distribution of the loading period and multiplying this volume concentration (see Table 2) with an assumed ammonium sulfate density of 1.77 g cm^{-3} (Haynes, 2014). The loading mass concentrations were in the range of 27.2 to 59.3 µg m^{-3} (see Table 2). The very narrow standard deviation around the mean particle number and volume size distribution in Figure 2 indicate clearly that the loading mass concentrations were very stable during the loading periods.

In the experiments ammonium sulfate filter loading areal densities were 3.1 to 99.6 mg m^{-2} in the case of the STAP and 1.2 to 15.9 mg m^{-2} in the case of the MA200. Exemplarily, PNSD and PVSD of the ammonium sulfate aerosol of the loading on Feb. 23 are shown in Figure 2. It is clearly visibly that the ammonium maximum in the particle volume size distribution peaked around a mobility diameter of 260 nm.

Figure 6 shows exemplarily the time series of the sample air *rh* and of the σ_{abs} measured with STAP and MA200 operated with clean filters. A *rh* of 0.0 to 96.2% with humidity change rates of -1.42 to 1.09 % s^{-1} was measured. Compared to the case in Figure 4 here a step-wise change of *rh* is shown. These steps resulted in a smaller absolute excursion of σ_{abs}

which ranges from -7.2 to 9.0 Mm^{-1} (STAP; 624 nm, 60 s measurement resolution) and -14.1 to 10.9 Mm^{-1} (MA200; 625 nm, 60 second running mean). Furthermore, Figure 6 shows the response of the σ_{abs} to *rh* changes at three different states of filter loading. During the first ramp the filter were clean, during the second period the filters had a filter areal loading density of 32.5 (STAP) and 12.4 (MA200) mg m^{-2} and during the third ramp the filter in the STAP had loading areal density of 98.7 mg m^{-2} and the MA200 filter was loaded with an areal loading density of 37.6 mg m^{-2}. The response of the instruments during these periods is shown in Appendixtable 1.

In Figure 5 (lower left panel), the overall (mean) response of both instruments to *rh* changes is shown in the case of loading with ammonium sulfate. The MA200 behaves similarly to the clean and BC case (slope of -0.40 Mm^{-1} $\%^{-1}$). The σ_{abs} measured by the STAP responses opposingly with a positive slope of 0.21 ± 0.01 Mm^{-1} $\%^{-1}$ which is roughly half the amplitude shown by the MA200 and around two thirds of the BC loaded case.

As shown in Figure 6, both absorption photometers measure an "apparent" absorption coefficient of approximately 2 Mm^{-1} during loading with ammonium sulfate (18:30 and 21:00 UTC). This shows that absorption photometers react sensitively to scattering aerosols such as ammonium sulfate. The scattering ability of any material can be described with the real part of its refractive index. It seems that for the STAP the slope of the correlation increases with increasing scattering of the loading material (0.15 Mm^{-1} $\%^{-1}$ for a clean filter, 0.21 Mm^{-1} $\%^{-1}$ for ammonium sulfate, and 0.30 Mm^{-1} $\%^{-1}$ for BC). Ammonium sulfate has a real part of 1.521 ± 0.002 (at 532 nm Dinar et al, 2007) and BC from combustion processes has a real part of 1.96 at 530 nm (Kim et al., 2015 following Ackermann and Toon (1981)). Hence, the quartz fiber glass filters loaded with "artificially" absorbing aerosol inside the STAP could lead to a variation in the response to relative humidity changes. But, the MA200 was loaded with ammonium sulfate as well and its response to relative humidity changes is almost constant for all considered loading materials. Therefore, either the observation is caused by the interaction of quartz fiber glass filters with the loading material and the PTFE filter inside the MA200 do not causes this behavior, the filter loading of the MA200 was too low, or there are other mechanisms explaining this. Furthermore, since only three different cases (clean, ammonium sulfate and BC) were observed in this study more materials should be considered to investigate this phenomenon. No correlation of linear regression slope and filter loading areal density ρ^* was observed in either case, for the STAP and the MA200, respectively. The slope (*a*) of STAP ranges from 0.17 Mm^{-1} $\%^{-1}$ to 0.24 Mm^{-1} $\%^{-1}$, and from -0.36 Mm^{-1} $\%^{-1}$ to -0.42 Mm^{-1} $\%^{-1}$ for the MA200. With a relative difference from minimum to maximum slope of 15.2 % the response of the MA200 is less variable than of the STAP with a relative variability of 28.6 % (slopes with $R^2 < 0.8$ excluded, all points included 36.8%). In Figure 7 (middle panel), the spread of the slopes within the shown cases is exemplarily shown for the investigated minimum and maximum load of the filters. Overall, the magnitude of the deviation of σ_{abs} was independent of the sigh of humidity change for both instruments.

3.3 Correction approach

The above chapters describe the overall behavior of the instruments to relative humidity changes averaging time of for 60 seconds. To correct for the described effect 1 Hz time resolution is needed to resolve the instantaneous response of the

instruments to relative humidity changes. For this purpose, a further laboratory experiment was conducted in which the inlets of both instruments could be flexibly exposed to humidified air. In our particular case, we hold the inlet into a beaker with a moistened tissue. In order to avoid any dampening bias, all measurements were conducted without particle filter in front of the inlet. But, during this experiment a background of about σ_{abs} of 1.2 Mm^{-1} was measured so that the filter loading was very low. First, we will consider the STAP and afterwards the MA200 is investigated.

3.3.1 STAP

In Figure 8 the correlation of *rh* change rate (d*rh*/d*t*) and the measured σ_{abs} at 624 nm measured by the STAP (red circles) and recalculated with respect to standard conditions (pressure of 1013.25 hPa and temperature 273.15 K) is shown. The STAP-based background eBC mass concentration during the experiment was ~190 ng m^3 (at standard conditions, σ_{abs} at 624 nm converted with a *MAC* of 6.6 m^2 g^{-1}), which corresponds to offset (standard conditions corrected values) in the shown scatterplot of Figure 8 and which has no influence on the response to *rh* changes as shown previously.

The *rh* change rate ranged from -10.8 to 14.5 % s^{-1}. These rates correspond to a σ_{abs} of -231 to 192 Mm^{-1} for recalculated values at standard conditions and -203 to 164 Mm^{-1} directly measured by the instrument. But these measurements are biased by the response time of the relative humidity sensor so that the "real" *rh* change-rate cannot fully represented by these measurements. On average the slope (correction factor C_{rh} in Eq. (8)) of the linear fit is 10.08 (± 0.12) Mm^{-1} s $\%^{-1}$ for standard conditions and 8.82 (± 0.10) Mm^{-1} s $\%^{-1}$ for direct instrument output, respectively. Calculating the particle light absorption coefficient introduced by *rh* changes with:

$$\sigma_{abs,rh} = C_{rh} \frac{drh}{dt}, \tag{8}$$

for different *rh* change rates in both, the recalculated and direct instrument output case, and subtracting it from measurements allows to correct for the observed effect as follows:

$$\sigma_{abs,corr} = \sigma_{abs,meas} - \sigma_{abs,rh}, \tag{9}$$

and after replacing $\sigma_{abs,rh}$ in Eq. (8) with Eq. (9) follows:

$$\sigma_{abs,corr} = \sigma_{abs,meas} - C_{rh} \frac{drh}{dt}. \tag{10}$$

The y-intersect of the linear fit in Figure 8 has not to be considered for correction as mentioned before. Disadvantageously, with this correction the noise of the *rh* sensor will propagate in the corrected σ_{abs}. Furthermore, the linear fit in Figure 8 under- or overestimates the behavior in regimes of very high relative humidity change rates most likely due to the response time of the *rh* sensor, so that the correction function cannot entirely correct the bias. Therefore, the given correction factor C_{rh} consists of uncertainties, which cannot be entirely addressed. Hence, it is only a first guess, needs further refinement and right now we do not recommend to use the correction approach as long the uncertainties are not fully addressed. Furthermore, since only one STAP was tested, other STAP may have other correction factors due to a unit to unit variability. Additionally, other filter

materials used in the STAP can also lead to another behavior. Anyhow, the upper function was applied to STAP measurements conducted with the same *rh* sensor under atmospheric conditions.

Exemplarily, Figure 9 shows this application. The figure shows airborne measurements of σ_{abs} at 624 nm derived with the STAP derived during a campaign conducted in March 2017 in East Germany. The upper panel displays the *rh* of a dried aerosol sample stream measured upstream of the STAP. The lower panel shows the recalculated σ_{abs} at 624 nm wavelength corrected for *rh* changes (black) and biased by *rh* changes (red). In the periods where the *rh* changes relatively fast (d*rh*/d*t* of -0.55 to 0.56 % s^{-1} e.g. at around 6200 seconds), the uncorrected σ_{abs} overshoots. The correction significantly reduces this bias and smooth out the measurements during the periods of *rh* changes. At the peaks of d*rh*/d*t* the difference of the corrected and uncorrected values is up to 1.5 Mm^{-1}, which is significant with respect to the measured $\sigma_{abs.}$ The periods with negative σ_{abs} are not introduced by the *rh* effect. We moreover think that a small offset is introduced in the initialization process of the instrument. Despite the imperfection of the correction scheme, this linear approach can be useful to derive a rough estimate of the accuracy of the measurements. For instance, let *x* be the required accuracy for the measurements in % and σ_{abs} the measured particle light absorption coefficient we can express the ambient particle light absorption coefficient which is at least needed to fulfill the accuracy criterion in dependency of the *rh* change rate d*rh*/d*t*:

$$\sigma_{\mathrm{abs,meas}} \geq \frac{100\%}{x[\%]} C_{\mathrm{rh}} \left[\frac{Mm^{-1}s}{\%}\right] \left|\frac{drh}{dt}\right| \left[\frac{\%}{s}\right]. \quad (11)$$

Exemplarily, if a change rate of 0.1 % s^{-1} is measured and an accuracy of 25% is needed, at least a measured particle light absorption coefficient of around 4 Mm^{-1} is needed to fulfill the accuracy criterion.

3.3.2 MA200

The exponential recovery behavior of the MA200 (see Figure 3) requires a more complex approach to correct for relative humidity changes. Therefore, the "apparent" particle light absorption coefficient can be described as a function of d*rh*/d*t* at a given time *t* ($\sigma_{abs,rh}(t)$):

$$\sigma_{\mathrm{abs,rh}}(t) = a\frac{drh}{dt}(t) + b\sigma_{\mathrm{abs,rh}}(t-1), \quad (12)$$

with *a* is a linear factor describing the dependency of $\sigma_{abs,rh}$ to d*rh*/d*t* and *b* is an exponential decay parameter between 0 and 1. The Eq. (12) corresponds to an autoregressive moving average model with exogenous variable (ARMA-X).

The function *marima* of the *R* package *marima* (v2.2) is capable to derive such an ARMA-X model (details in Appendix A). From this the coefficients *a* and *b* can be derived. These can be furthermore used as initial parameters for an optimization by minimizing the sum of the squared residual errors. The derived ARMA-X model describes σ_{abs}(d*rh*/d*t*) as follows:

$$\sigma_{\mathrm{abs,rh}}(t) = -0.47\left[\frac{Mm^{-1}s}{\%}\right]\frac{drh}{dt}(t) + 0.93\sigma_{\mathrm{abs,rh}}(t-1), \quad (13)$$

and with the applied optimization:

$$\sigma_{\mathrm{abs,rh}}(t) = -0.50\left[\frac{Mm^{-1}s}{\%}\right]\frac{drh}{dt}(t) + 0.96\sigma_{\mathrm{abs,rh}}(t-1). \quad (14)$$

Figure 10 shows time series of *rh* (upper panel) and 60 s running average σ_{abs} derived with the MA200 at 625 nm with 1 Hz time resolution derived during the laboratory experiment mentioned in 3.4. Under the influence of d*rh*/d*t* in the range of -11.2 to 17.1 % s^{-1} the 60 s running average of σ_{abs} is between -6.5 to 7.7 Mm^{-1} (M_{eBC} equivalent of -0.99 to 1.20 µg m^{-3}). Subtracting the calculated "apparent" particle light absorption coefficient in dependency of *rh* changes following Eq. (13) and (14) to this data set σ_{abs} shrinks to -3.2 to 4.7 Mm^{-1} or -1.0 to 3.7 Mm^{-1} in the non- and optimized case, respectively. This corresponds to M_{eBC} of around -0.5 to 0.7 µg m^{-3}, or -0.2 to 0.6 µg m^{-3} in the optimized case. This indicates, that the presented approach can significantly reduce the *rh* bias in the presented case. But, *rh* change induced fluctuations in σ_{abs} are still visible, which indicates that correction scheme cannot account entirely for all the bias introduced by a change in *rh*. Here, the response time of the sensor could account at least for a part of the imperfection of the correction approach and cannot be fully quantified, yet.

Unfortunately, the application of the same correction approach to other similar experiments resulted in different correction function *a* and *b*. Applying the approach to two clean case experiments from section 3.1 resulted in optimized parameters of *a* = -0.92 and -1.03 and *b* = 0.974 and 0.971, respectively. Hence, it is just a first step trying to account for relative humidity changes and further research with more MA200 simultaneously has to be done to fully understand the underlying processes and to fully quantify the uncertainties of the correction scheme Nevertheless, the presented approach significantly reduces the amplitude of the bias in the shown data set (see Figure 10). But, up to now we cannot recommend to use the given parameters to correct for *rh* effects. At most it can be used to make a rough estimate of how measurements of the particle light absorption coefficient derived the MA200 could be biased by *rh* changes.

6 Summary and Conclusion

Here we presented a unique set of laboratory studies to investigate the response of two different types of filter-based absorption photometers (STAP and MA200) with different filter material (quartz-fiber glass, and PTFE) to relatively fast changes in relative humidity of sampled aerosol. Different filter loading densities with different loading material (clean, black carbon, and ammonium sulfate) where considered in this study. Both instruments revealed that they react to fast humidity changes but in opposite ways, induced by the different filter material. This opposing behavior could be a chance to design an instrument on the basis of both filter materials so that the effects cancel out each other. No significant differences between the loading aerosol types were observed in the case of the MA200, whereas the STAP revealed the strongest response in the BC case.

The MA200 revealed a very robust response of -0.42 to -0.36 Mm^{-1} $\%^{-1}$ (negative excursion of σ_{abs} with increasing *rh*), whereas the STAP was more fluctuating across loading areal density and loading aerosol type with a positive excursion of σ_{abs} in the range of 0.17 to 0.62 Mm^{-1} $\%^{-1}$. We assume that in the case of the MA200 it is more a filter effect, or the filter loadings were too low to have a significant effect due to the lower volume flow rate. For the STAP, more parameters could

also have an effect and further investigation is needed. For loading areal density on the filter no correlation was found, although we expected that the hygroscopic ammonium sulfate will affect the transmissivity of the filter-aerosol layer. Hence, we think excursions of σ_{abs} due to relative humidity changes is mainly caused by water vapor filter material interactions and is independent of the filter loading areal density or they were too low to observe significant effects.

Furthermore, we developed some correction approaches for both instruments to account for fast *rh* changes. For the STAP a linear correction function was derived. This correction follows a linear approach including a correction factor of C_{rh} = 10.08 ± 0.12 Mm^{-1} s $\%^{-1}$ for standard conditions and 8.82 ± 0.10 Mm^{-1} s $\%^{-1}$ for direct instrument output without any corrections. But this correction was created with a *rh* sensor with a response time which introduces a bias in the correction approach and cannot be quantified, yet. Also, other *rh* sensors might result in a different correction formula. Exemplarily, this correction was applied to an airborne data set and has shown promising results. For the MA200 no linear correction function can be provided, since after an excursion of σ_{abs} the MA200 shows a distinct exponentially behaving recovery function. Therefore, an ARMA-X model was developed to account for this exponential decay and to describe the σ_{abs} in dependency of d*rh*/d*t*. Applying this to the presented data set, this significantly reduced the excursion introduced by *rh* changes. We do not recommend to use the presented approaches, since the uncertainties cannot be fully quantified yet and a refinement is need on the base of more experiments to fully understand the underlying processes and to quantify the uncertainties. The findings summarized above lead to following recommendations how to use this type of instruments:

1. When used for vertical profiling, apparent sharp gradients in *rh* during the profile have to be considered.
    a. The ascending speed of the profiling platform should be reduced if possible, to decrease the temporal change of *rh*, but in some scenarios this is simply not possible and therefore,
    b. when fast relative humidity changes cannot be avoided, such periods have to be removed from the data set, or at least to estimate the uncertainties of the measurements based on the presented correction functions. Therefore,
2. we recommend recording the *rh* of the sampled aerosol. This allows to determine *rh* change rates. This allows to roughly estimate the bias of *rh* changes on filter-based absorption measurements with these two instruments.
3. The usage of a dryer is highly recommended, because it reduces the amplitude of the excursion in the measurements during fast *rh* changes.
4. For both instruments we recommend to conduct more similar experiments to address the flaws of our study to refine the presented correction approaches.
5. Since the response is different in magnitude and sign for both filter materials, we recommend to examine the effect for other filter materials as well.

Appendix A: Multivariate Autoregressive Integrated Moving Average model with exogenous variable – MARIMA-X

The multivariate autoregressive integrated moving average model with exogenous variable (MARIMA-X(p,d,q)) can model the behavior of an observation driven by an exogenous variable. It consists of three parts, the autoregressive (AR) part of order p, the moving average (MA) part of order q, and the integrating (I) part, which describes how often (*d* times) a time series has to be differentiated to be stationary. An MARIMA-X model can be described as:

$$Y_t = aX_t + b_1Y_{t-1} + b_2Y_{t-2} + \ldots + b_nY_{t-n} + \dot{o}_t + c_2\dot{o}_{t-2} + c_1\dot{o}_{t-1} + \ldots + c_n\dot{o}_{t-n}, \quad \text{(A1)}$$

with Y_t the predicted value of the model at the time *t*. b_1Y_{t-1} to b_nY_{t-n} are part of the autoregressive module of the model, with the corresponding coefficients b_1 to b_n, describing the contribution of each Y_{t-n} to Y_t. X_t represents the corresponding independent exogenous variable at time *t*, whereas the ϵ_t are part of the moving average of the model, which accounts for lagged error terms, ϵ_t introduced by the model itself. c_1 to c_n indicate the contribution of ϵ_t to ϵ_{t-n} to Y_t. For predictions of a variable the error term is unknown. A special case of the MARIMA-X model is the MARMA-X model or ARMA-X, in which the integrating part has an order of 0. Detailed information about ARIMA models can be found in Durbin and Koopman (2012) and Lütkepohl (2005). A tutorial to estimate MARIMA models in *R* is provided by Spliid (2016).

Appendix B: Table with overview of all investigated cases

Acknowledgements

We would like to thank Dr. Sascha Pfeiffer very much for his guidance in setting up the experiment and for the introduction to the particle generators. We would also like to express our sincere thanks to Ralf Käthner for his valuable support with data acquisition troubleshooting.

Code/Data availability

Any used code and the data can be requested via the given corresponding E-mail address.

Author contribution

Conceptualization: Sebastian Düsing and Thomas Müller; Data curation: Sebastian Düsing; Investigation: Sebastian Düsing; Methodology: Sebastian Düsing; Software, Sebastian Düsing and Almond Stöcker; Supervision, Thomas Müller, Birgit Wehner, Almond Stöcker, and Alfred Wiedensohler; Visualization: Sebastian Düsing; Writing – original draft, Sebastian Düsing; Writing – review & editing: Sebastian Düsing, Thomas Müller, Birgit Wehner, and Almond Stöcker.

Competing interested

We, the authors, declare no conflict of interests.

References

Ackerman, T. P., and Toon, O. B.: Absorption of Visible Radiation in Atmosphere Containing Mixtures of Absorbing and Non-Absorbing Particles, Appl. Opt., 20, 3661–3668, 1981.

Alas, H.D., Müller, T., Birmili, W., Kecorius, S., Cambaliza, M.O., Simpas, J.B.B., Cayetano, M., Weinhold, K., Vallar, E., Galvez, M.C. and Wiedensohler, A.: Spatial characterization of black carbon mass concentration in the atmosphere of a Southeast Asian megacity: An air quality case study for Metro Manila, Philippines. Aerosol Air Qual. Res. 18: 2301–2317, 2018.

Bärfuss, Konrad; Pätzold, Falk; Altstädter, Barbara; Kathe, Endres; Nowak, Stefan; Bretschneider, Lutz; Bestmann, Ulf; Lampert, Astrid: New Setup of the UAS ALADINA for Measuring Boundary Layer Properties, Atmospheric Particles and Solar Radiation. In: Atmosphere 9, p. 28, 2018.

B+B Thermo-Technik GmbH, HYT-939 data-sheet, url: https://shop.bb-sensors.com/out/media/Datasheet_digital_humidity_sensor_HYT939.pdf, 2015

Birmili, W., Weinhold, K., Rasch, F., Sonntag, A., Sun, J., Merkel, M., Wiedensohler, A., Bastian, S., Schladitz, A., Löschau, G., Cyrys, J., Pitz, M., Gu, J., Kusch, T., Flentje, H., Quass, U., Kaminski, H., Kuhlbusch, T. A. J., Meinhardt, F., Schwerin, A., Bath, O., Ries, L., Gerwig, H., Wirtz, K., and Fiebig, M.: Long-term observations of tropospheric particle number size distributions and equivalent black carbon mass concentrations in the German Ultrafine Aerosol Network (GUAN), Earth Syst. Sci. Data, 8, 355-382, https://doi.org/10.5194/essd-8-355-2016, 2016.

T. C. Bond, T. L. Anderson & D. Campbell: Calibration and Intercomparison of Filter-Based Measurements of Visible Light Absorption by Aerosols, AerosolScience & Technology, 30:6, 582-600, DOI: 10.1080/027868299304435, 1999.

T. C. Bond, S. J. Doherty, D. W. Fahey, P. M. Forster, T. Berntsen, B. J. DeAngelo, M. G. Flanner, S. Ghan, B. Kärcher, D. Koch, S. Kinne, Y. Kondo, P. K. Quinn, M. C. Sarofim, M. G. Schultz, M. Schulz, C. Venkataraman, H. Zhang, S. Zhang, N. Bellouin, S. K. Guttikunda, P. K. Hopke, M. Z. Jacobson, J. W. Kaiser, Z. Klimont, U. Lohmann, J. P. Schwarz, D. Shindell, T. Storelvmo, S. G. Warren, C. S. Zender (2013), Bounding the role of black carbon in the climate system: A scientific assessment, J. Geophys. Res. Atmos., 118, 5380–5552, doi:10.1002/jgrd.50171, 2013.

Cai, J., Yan, B., Ross, J., Zhang, D., Kinney, P. L., Perzanowski, M. S., Chillrud, S. N.: Validation of microAeth® as a black carbon monitor for fixed-site measurement and optimization for personal exposure characterization. Aerosol and Air Quality Research, 14(1), 1–9. https://doi.org/10.4209/aaqr.2013.03.0088, 2014.

Caroll, B. J.: The accurate measurement of contact angle, phase contact areas, drop volume, and Laplace excess pressure in drop-on-fiber systems, J. Coll. Interface Sci., 57(3), 488-495, 1976.

Caroll, B. J.: Equilibrium conformations of liquid drops on thin cylinders under forces of capillarity. A theory for the roll-up process., Langmuir, 2(2), 248-250, 1986.

Cepeda, M., Schoufour, J., Freak-Poli, R., Koolhaas, C., Dhana, K., Bramer, W. and Franco, O.: Levels of ambient air pollution according to mode of transport: a systematic review. *The Lancet Public Health*, 2(1), pp.e23-e34, 2017.

Dinar, E., Abo Riziq, A., Spindler, C., Erlick, C., Kiss, G., & Rudich, Y.: The complex refractive index of atmospheric and model humic-like substances (HULIS) retrieved by a cavity ring down aerosol spectrometer (CRD-AS), Faraday Discussions, 137, 275-295, https://doi.org/10.1039/b703111d, 2007.

Durbin, J. and Koopman, S.: Time series analysis by state space methods. Oxford: Oxford University Press, 2012.

Ferrero, L., Castelli, M., Ferrini, B. S., Moscatelli, M., Perrone, M. G., Sangiorgi, G., D'Angelo, L., Rovelli, G., Moroni, B., Scardazza, F., Močnik, G., Bolzacchini, E., Petitta, M., and Cappelletti, D.: Impact of black carbon aerosol over Italian basin valleys: high-resolution measurements along vertical profiles, radiative forcing and heating rate, Atmos. Chem. Phys., 14, 9641-9664, https://doi.org/10.5194/acp-14-9641-2014, 2014

Ferrero, L., Cappelletti, D., Busetto, M., Mazzola, M., Lupi, A., Lanconelli, C., Becagli, S., Traversi, R., Caiazzo, L., Giardi, F., Moroni, B., Crocchianti, S., Fierz, M., Močnik, G., Sangiorgi, G., Perrone, M. G., Maturilli, M., Vitale, V., Udisti, R., and Bolzacchini, E.: Vertical profiles of aerosol and black carbon in the Arctic: a seasonal phenomenology along 2 years (2011–2012) of field campaigns, Atmos. Chem. Phys., 16, 12601-12629, https://doi.org/10.5194/acp-16-12601-2016, 2016.

Haynes, W.M. (ed.). CRC Handbook of Chemistry and Physics. 95th Edition. CRC Press LLC, Boca Raton: FL 2014-2015, 2014.

Holder, A., B. Seay, A. Brashear, T. Yelverton, J. Blair, and S. Blair. Evaluation of a multi-wavelength black carbon sensor, Poster, 10th International Aerosol Conference, St. Louis, MO, September 02 - 07, url: https://cfpub.epa.gov/si/si_public_record_report.cfm?Lab=NRMRL&dirEntryId=342614, 2018.

IPCC: Cubasch, U., D. Wuebbles, D. Chen, M.C. Facchini, D. Frame, N. Mahowald and J.-G. Winther: Introduction. In: Climate Change 2013: The Physical Science Basis. Contribution of Working Group I to the Fifth Assessment Report of the Intergovernmental Panel on Climate Change [Stocker, T.F., D. Qin, G.-K. Plattner, M. Tignor, S.K. Allen, J. Boschung, A. Nauels, Y. Xia, V. Bex and P.M. Midgley (eds.)]. Cambridge University Press, Cambridge, United Kingdom and New York, NY, USA, 119–158, doi:10.1017/CBO9781107415324.007., 2013.

Jing, L.: Standard Combustion Aerosol Generator for Calibration Purposes. 3rd ETH Conference on Combustion Generated Nanoparticles. Zurich, 9–10 August, 1999.

Kim, J., Bauer, H., Dobovičnik, T., Hitzenberger, R., Lottin, D., Ferry, D., & Petzold, A.: Assessing optical properties and refractive index of combustion aerosol particles through combined experimental and modeling studies. Aerosol Science and Technology, 49(5), 340-350, https://doi.org/10.1080/02786826.2015.1020996, 2015.

Lack, D. A., Cappa, C. D., Covert, D. S., Baynard, T., Massoli, P., Sierau, B., Bates, T. S., Quinn, P. K., Lovejoy, E. R., & Ravishankara, A. R.: Bias in Filter-Based Aerosol Light Absorption Measurements Due to Organic Aerosol Loading: Evidence from Ambient Measurements, Aerosol Science and Technology, 42:12, 1033-1041, DOI: 10.1080/02786820802389277, 2008.

Lütkepohl H.: Introduction To Multiple Time Series Analysis, Berlin: Springer-Verlag; 2005.

Markowicz, K. M., Ritter, C., Lisok, J., Makuch, P., Stachlewska, I. S., Cappelletti, D., Chilinski, M. T.: Vertical variability of aerosol single-scattering albedo and equivalent black carbon concentration based on in-situ and remote sensing techniques during the iAREA campaigns in Ny-Ålesund. Atmospheric Environment. https://doi.org/10.1016/j.atmosenv.2017.06.014, 2017.

Nessler, R., Sheridan, P.J., Ogren, J.A., Weingartner, E., and Hannemann, A.: Effect of humidity on filter-based measurements of the aerosol light absorption. NOAA ESRL GLOBAL MONITORING ANNUAL CONFERENCE, 2006.

Ogren, J. A., Wendell, J., Andrews, E., and Sheridan, P. J.: Continuous light absorption photometer for long-term studies, Atmos. Meas. Tech., 10, 4805-4818, https://doi.org/10.5194/amt-10-4805-2017, 2017.

Ogren, J.A.: Comment on “Calibration and Intercomparison of Filter-Based Measurements of Visible Light Absorption by Aerosols”, Aerosol Science and Technology, 44:8, 589-591, DOI: 10.1080/02786826.2010.482111, 2010.

Petzold, A. and M. Schönlinner: Multi-angle absorption photometry – a new method for the measurement of aerosol light absorption and atmospheric black carbon, *J. Aerosol Sci.*, 35, 421-441, 2004.

Petzold, A., Ogren, J. A., Fiebig, M., Laj, P., Li, S.-M., Baltensperger, U., Holzer-Popp, T., Kinne, S., Pappalardo, G., Sugimoto, N., Wehrli, C., Wiedensohler, A., and Zhang, X.-Y.: Recommendations for reporting "black carbon" measurements, Atmos. Chem. Phys., 13, 8365-8379, https://doi.org/10.5194/acp-13-8365-2013, 2013.

Ran, L., Deng, Z., Xu, X., Yan, P., Lin, W., Wang, Y., Tian, P., Wang, P., Pan, W., and Lu, D.: Vertical profiles of black carbon measured by a micro-aethalometer in summer in the North China Plain, Atmos. Chem. Phys., 16, 10441–10454, https://doi.org/10.5194/acp-16-10441-2016, 2016.

Rosati, B., Herrmann, E., Bucci, S., Fierli, F., Cairo, F., Gysel, M., Tillmann, R., Größ, J., Gobbi, G. P., Di Liberto, L., Di Donfrancesco, G., Wiedensohler, A., Weingartner, E., Virtanen, A., Mentel, T. F., and Baltensperger, U.: Studying the vertical aerosol extinction coefficient by comparing in situ airborne data and elastic backscatter lidar, Atmos. Chem. Phys., 16, 4539-4554, https://doi.org/10.5194/acp-16-4539-2016, 2016.

Spliid, H.: Multivariate Time Series Estimation using marima. In . P. Linde (Ed.), Symposium i anvendt statistik 2016 (pp. 108-123). Danmarks Statistik, 2016.

Subramanian, R., Roden, C. A., Boparai. P., and Bond, T. C.: Yellow Beads and Missing Particles: Trouble Ahead for Filter-Based Absorption Measurements, Aerosol Sci. Technol. 41:6, 630–637, https://doi.org/10.1080/02786820701344589, 2007.

Telg, H., Murphy, D. M., Bates, T. S., Johnson, J. E., Quinn, P. K., Giardi, F., and Gao, R.: A practical set of miniaturized instruments for vertical profiling of aerosol physical properties, Aerosol Science and Technology, 51:6, 715-723, DOI: 10.1080/02786826.2017.1296103, 2017.

Vecchi, R., Bernardoni, V., Paganelli, C., and Valli, G..: A filter-based light-absorption measurement with polar photometer: Effects of sampling artefacts from organic carbon, Journal of Aerosol Science., 70, 4805-4818, https://doi.org/10.1016/j.jaerosci.2013.12.012, 2013.

Wiedensohler, A., Birmili, W., Nowak, A., Sonntag, A., Weinhold, K., Merkel, M., Wehner, B., Tuch, T., Pfeifer, S., Fiebig, M., Fjäraa, A. M., Asmi, E., Sellegri, K., Depuy, R., Venzac, H., Villani, P., Laj, P., Aalto, P., Ogren, J. A., Swietlicki, E., Williams, P., Roldin, P., Quincey, P., Hüglin, C., Fierz-Schmidhauser, R., Gysel, M., Weingartner, E., Riccobono, F., Santos, S., Grüning, C., Faloon, K., Beddows, D., Harrison, R., Monahan, C., Jennings, S. G., O'Dowd, C. D., Marinoni, A., Horn, H.-

G., Keck, L., Jiang, J., Scheckman, J., McMurry, P. H., Deng, Z., Zhao, C. S., Moerman, M., Henzing, B., de Leeuw, G., Löschau, G., and Bastian, S.: Mobility particle size spectrometers: harmonization of technical standards and data structure to facilitate high quality long-term observations of atmospheric particle number size distributions, Atmos. Meas. Tech., 5, 657-685, https://doi.org/10.5194/amt-5-657-2012, 2012.

World Health Organization (European Office): Health Effects of Black Carbon. Copenhagen, Denmark: WHO, ISBN: 9789289002653 2012.

WMO/GAW: Aerosol measurement procedures guidelines and recommendations 2nd edition, GAW Rep. 227, World Meteorol. Organ., Geneva, Switzerland, https://library.wmo.int/doc_num.php?explnum_id=3073, 2016.

Zarzycki, C. and Bond, T. C.: How much can the vertical distribution of black carbon affect its global direct radiative forcing?, Geophysical Research Letters - GEOPHYS RES LETT. 37. 10.1029/2010GL044555, 2010.

Table and figures

Table 1: Filter loading mass concentration (M_{eBC}) of the black carbon particles and filter areal loading density (deposited mass per spot area) ρ^*_i. M_{eBC} were determined by dividing the average σ_{abs} of the STAP with an assumed *MAC* of 6.6 $m^2\ g^{-1}$ or based on the MAAP measurements. Usage of same filter is indicated by a separation with thick horizontal lines. Bold written entries were used for the investigation of the *rh* effect.

filter number	M_{eBC} [µg m^{-3}]	$\rho^*_{eBC,i}$ [mg m^{-2}]	
		STAP	**MA200**
#1	**44.5 (STAP)**	**14.0**	**5.4**
	43.4 (STAP)	37.9	14.4
	27.6 (STAP)	**42.9**	**16.3**
#2	**52.6 (MAAP, 2 scans)**	**2.8**	**1.1**
#3	-	**13.7 (integral of STAP)**	no data

Table 2: Average volume and mass concentration ($V_{(NH4)2SO4}$, $M_{(NH4)2SO4}$) of the loading $(NH_4)_2SO_4$ aerosol derived from the used MPSS (number of used scans in brackets) and loading areal density $\rho^*_{(NH4)2SO4}$ of the filters are given. Usage of same filter is indicated by a separation with thick horizontal lines, which means that the filter loading mass was adding up during the experiments.

filter number	$V_{(NH4)2SO4}$ [µm^3 cm^{-3}] (# scans)	$M_{(NH4)2SO4}$ [µg m^{-3}]	$\rho^*_{(NH4)2SO4}$ [mg m^{-2}]	
			STAP	**MA200**
#1	15.4 (2)	27.2	3.1	1.2
	18.6 (1)	32.9	10.5	4.0
	20.6 (3)	36.4	31.3	11.9
#2	20.6 (4)	36.5	40.8	15.5
#3	33.1 (3)	58.6	32.5	12.4
	33.5 (5)	59.3	98.7	37.6
#4	20.3 (3)	36.0	21.1	8.0
	20.3 (3)	36.0	41.9	15.9
#5	23.9 (3)	42.4	28.9	no data
	28.4 (4)	50.2	69.8	no data
	29.8 (2)	52.8	99.6	no data

Appendixtable 1: Coefficients of the linear regression of the instrument response to *rh* changes (*a* is slope, *b* is y-intersect, and R^2 the correlation coefficient) for the clean, ammonium sulfate and BC case for different loading areal densities ρ^*_i. The number of data-points is represented by *n*. Bold written entries represent cases with a R^2 larger than 0.8. σ indicates the standard deviation of the fitting parameters. For ammonium sulfate τ not considered.

loading aerosol	device	ρ^*_i [mg m^{-2}]	τ	*n*	*a* [Mm^{-1} %$^{-1}$]	$\sigma(a)$ [Mm^{-1} %$^{-1}$]	*b* [Mm^{-1}]	$\sigma(b)$ [Mm^{-1}]	R^2
clean	**MA200 (625 nm)**	**-**	**-**	**147**	**-0.41**	**0.00**	**-0.28**	**0.10**	**0.99**
	STAP (624 nm)	-	-	241	0.14	0.00	0.44	0.12	0.79
BC	**MA200 (625 nm)**	**1.1**	**0.98**	**18**	**-0.42**	**0.02**	**0.11**	**0.18**	**0.97**
		5.3	**0.95**	**9**	**-0.40**	**0.03**	**0.38**	**0.24**	**0.96**
		16.3	**0.82**	**9**	**-0.37**	**0.03**	**0.54**	**0.24**	**0.95**
	MA200 (625 nm, all)	**-**	**-**	**36**	**-0.41**	**0.01**	**0.28**	**0.12**	**0.96**
	STAP (624 nm)	2.8	0.93	13	0.17	0.05	0.14	0.52	0.47
		13.7	**0.78**	**33**	**0.29**	**0.01**	**1.26**	**0.37**	**0.94**
		14.0	0.74	10	0.38	0.19	0.89	1.49	0.25
		42.9	0.52	10	0.62	0.32	1.64	2.54	0.23
	STAP (624 nm, all)	-	-	66	0.29	0.02	1.00	0.48	0.72
$(NH_4)_2SO_4$	**MA200 (625 nm)**	**1.1**	**-**	**9**	**-0.38**	**0.04**	**0.39**	**0.31**	**0.93**
		4.0	**-**	**10**	**-0.42**	**0.04**	**0.00**	**0.27**	**0.94**
		8.0	**-**	**41**	**-0.41**	**0.01**	**0.10**	**0.13**	**0.97**
		11.9	**-**	**10**	**-0.40**	**0.03**	**-0.21**	**0.24**	**0.95**
		12.4	**-**	**15**	**-0.39**	**0.01**	**0.25**	**0.16**	**0.99**
		15.5	**-**	**9**	**-0.37**	**0.03**	**0.47**	**0.23**	**0.95**
		15.9	**-**	**18**	**-0.42**	**0.02**	**0.07**	**0.20**	**0.98**
		37.6	**-**	**15**	**-0.36**	**0.02**	**0.04**	**0.21**	**0.97**
	MA200 (625 nm, all)	**-**	**-**	**127**	**-0.40**	**0.01**	**0.10**	**0.07**	**0.97**
	STAP (624 nm)	3.1	-	10	0.17	0.09	0.35	0.72	0.23
		10.5	-	10	0.19	0.09	0.33	0.72	0.28
		21.1	-	34	0.20	0.04	0.73	0.49	0.42
		28.9	**-**	**90**	**0.23**	**0.01**	**0.92**	**0.34**	**0.81**
		31.3	-	10	0.19	0.09	0.34	0.71	0.28
		32.5	**-**	**13**	**0.19**	**0.02**	**0.35**	**0.36**	**0.82**
		40.8	-	10	0.21	0.10	0.42	0.79	0.28
		41.9	-	16	0.20	0.05	0.16	0.64	0.47
		69.8	**-**	**56**	**0.19**	**0.01**	**0.89**	**0.16**	**0.96**
		98.7	**-**	**14**	**0.24**	**0.03**	**0.28**	**0.39**	**0.86**
		99.6	**-**	**33**	**0.19**	**0.01**	**0.87**	**0.24**	**0.95**
	STAP (624 nm, all)	**-**	**-**	**296**	**0.21**	**0.01**	**0.71**	**0.14**	**0.82**

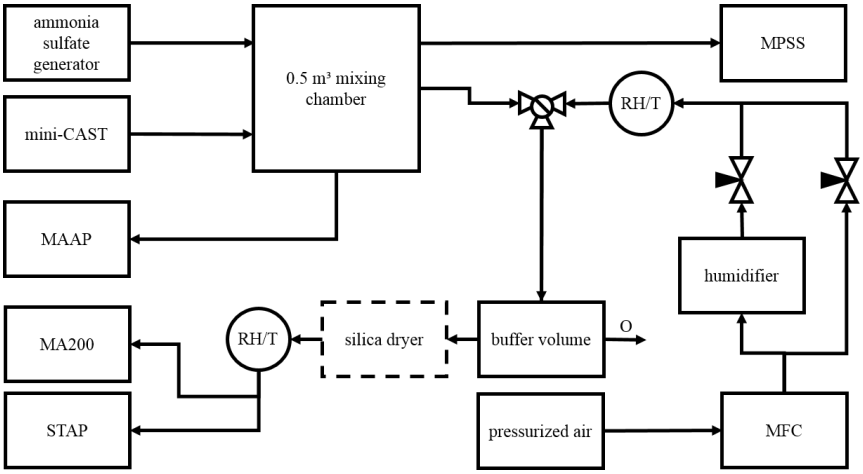

Figure 1: Scheme of the experimental setup. The volumetric flow rates of two air-streams were controlled with two needle valves to produce humidified particle free air via mixing of wet and dry particle free air. It was ensured that the sum of both flows was larger than the volumetric flow of both absorption photometer investigated here. Any exceeding airflow was directed to a buffer volume with an overflow outlet (O). The relative humidity and the temperature of the air were recorded directly after the humidifier and shortly before the photometers with the *rh* and *T* sensors.

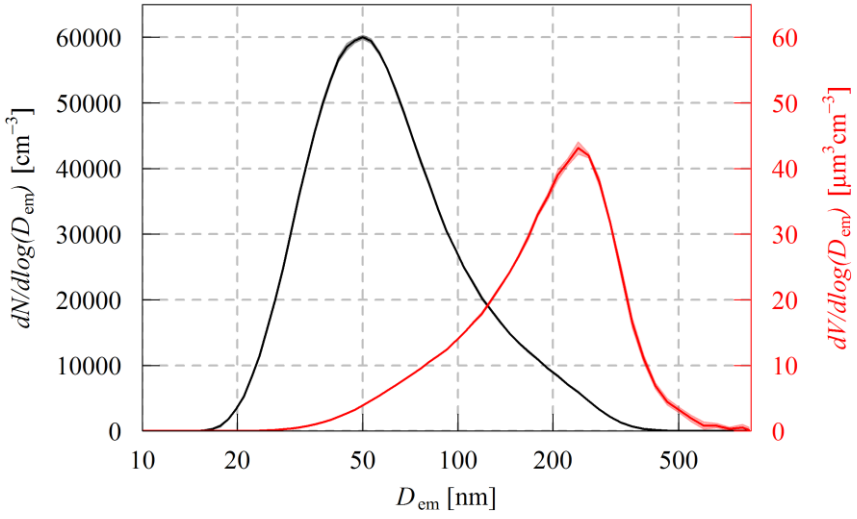

Figure 2: Average particle number (black) and volume size distributions (red) of the ammonium sulfate aerosol loaded on the filters in the MA200 and STAP during experiment #2 of the ammonium sulfate loading experiments. The average volume of 20.6 µm³ cm⁻³ is calculated from four scans. The shaded area indicate the standard deviation of the mean. D_{em} refers herein to the electrical mobility diameter of the aerosol particles.

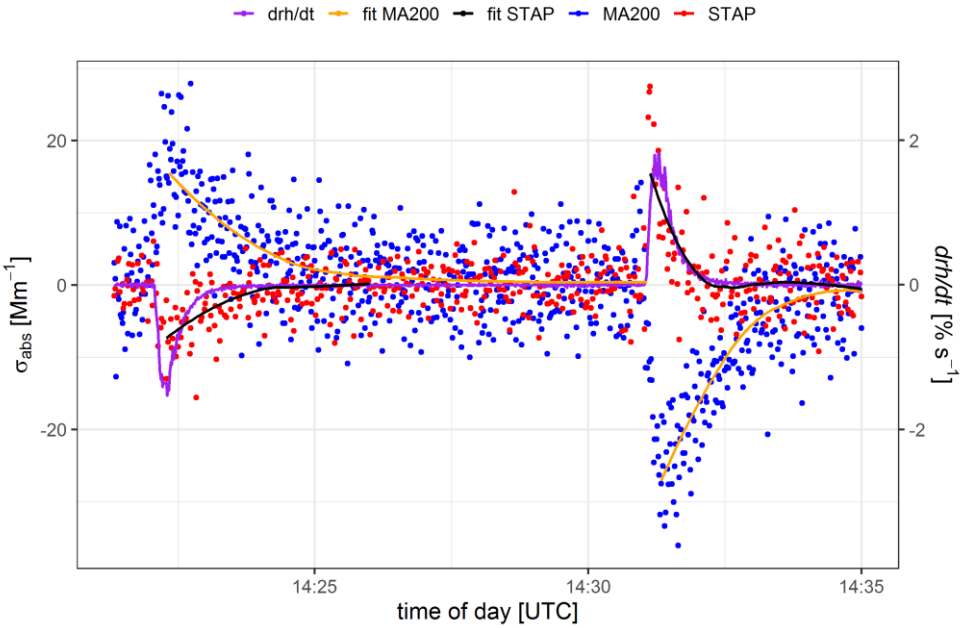

Figure 3: 1 Hz raw data of σ_{abs} at 625 nm measured by the MA200 (blue points) and recalculated at 624 nmSTAP200 (red points), the smooth fit through the measurements (orange and black), and d*rh*/d*t* (purple line).

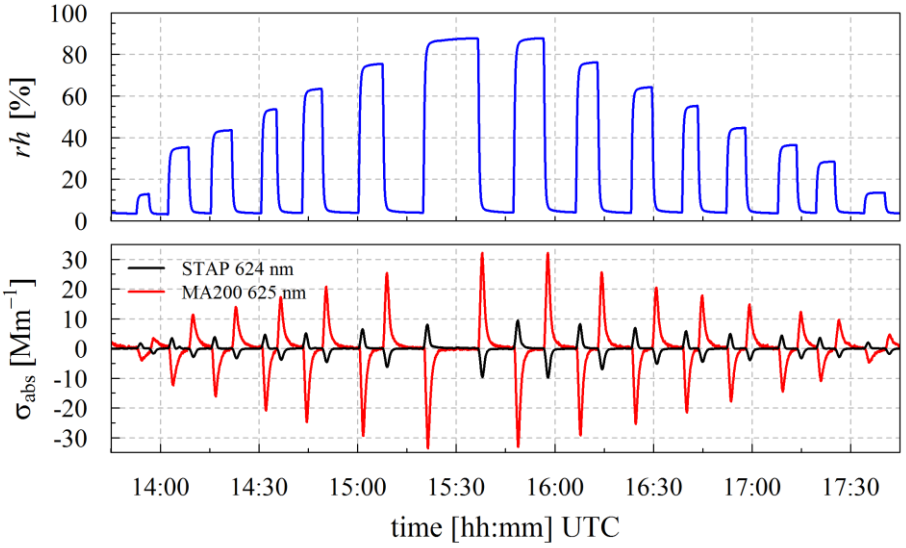

Figure 4: Time series of *rh* (top panel) and absorption coefficient (bottom panel) measured with STAP (624 nm; black) and MA200 (625 nm; red) with clean filters.

670

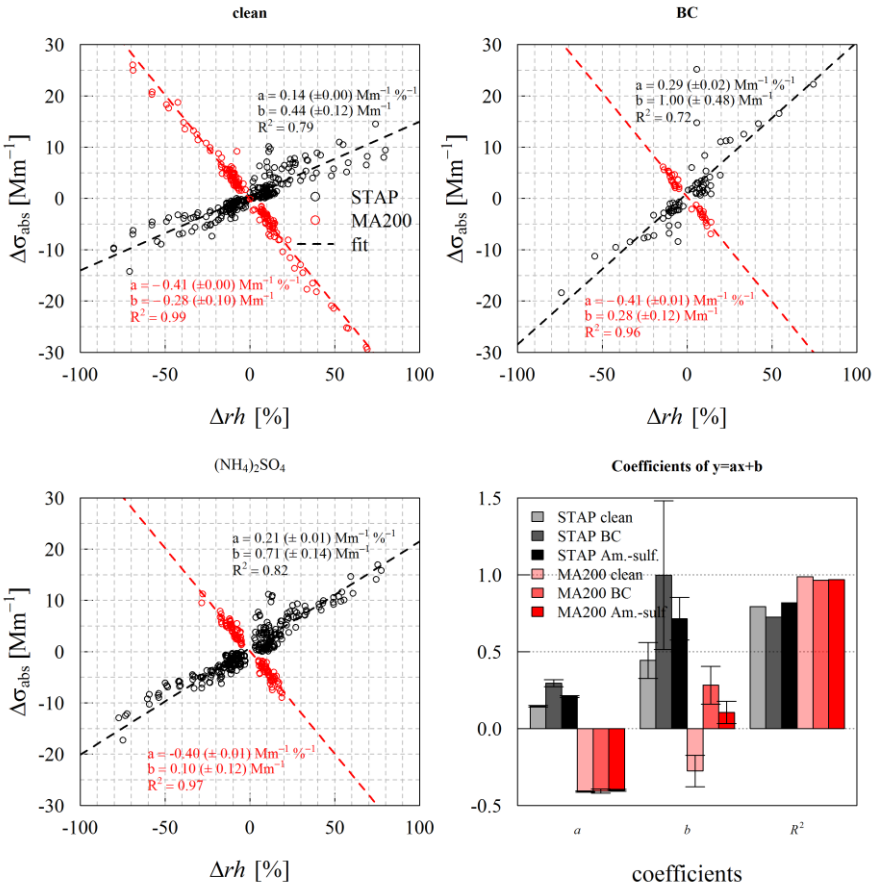

Figure 5: Scatter plot (dots) of all observations of the absolute excursion of σ_{abs} ($\Delta\sigma_{abs}$) in dependence of the absolute change in *rh* (Δ*rh*), its linear regression fit as well as the summarizing boxplot of the linear regression fit are shown for the three investigated states (clean, loaded with BC and ammonium sulfate) at 624 nm (STAP, black colors) and 625 nm (MA200, red colors). Descriptive coefficients are given in Appendixtable 1.

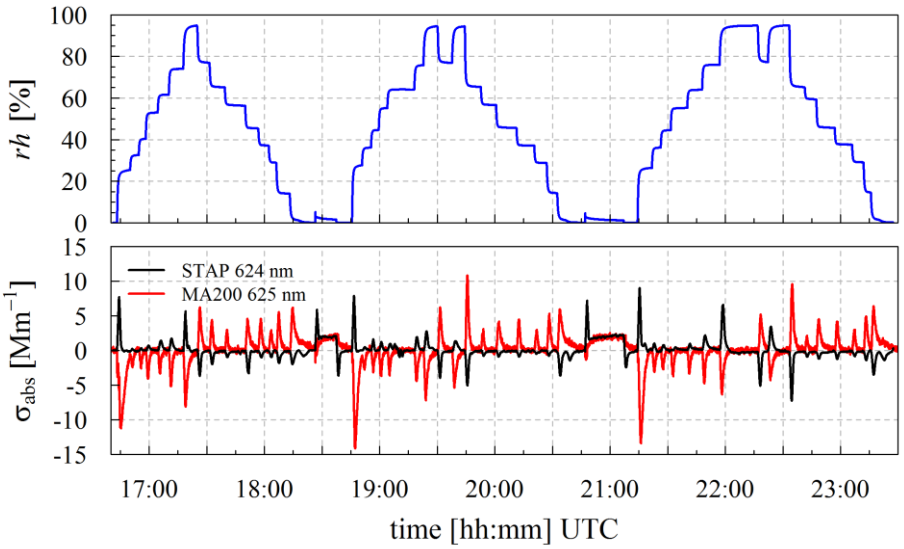

Figure 6: *rh* of the air stream sampled by the MA200 and the STAP (upper panel) and σ_{abs} measured by MA200 and STAP at 625 (624) nm (lower panel). First up and down ramp of *rh* conducted with clean filter, second and third under conditions with filter loaded with ammonium sulfate. Loading periods around 18:30 and 21:00 UTC.

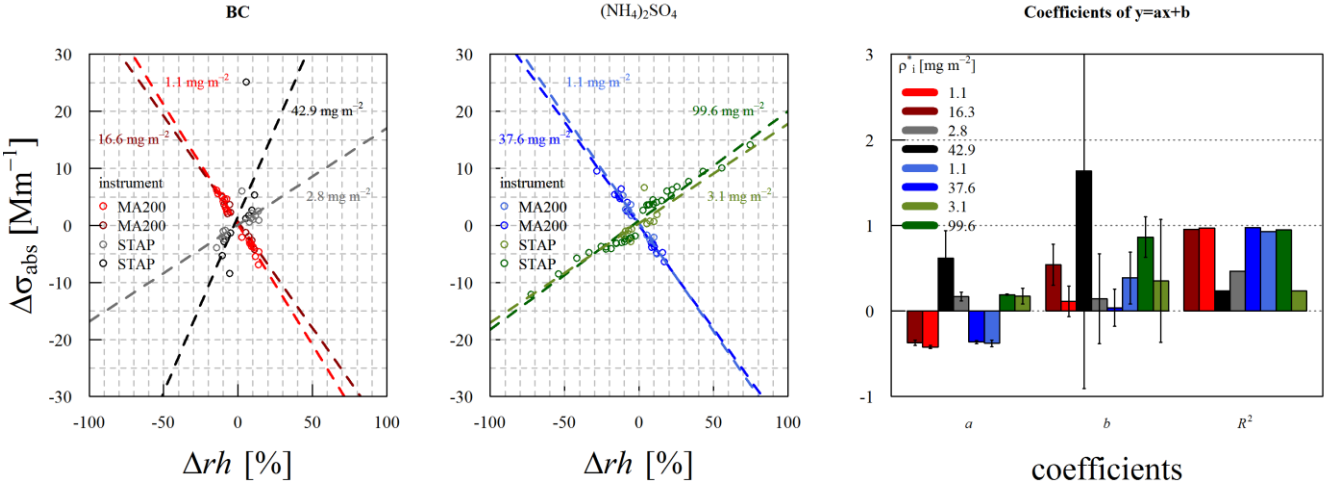

Figure 7: Scatter plot of change in absorption ($\Delta\sigma_{abs}$) in dependence of the absolute change in *rh* (Δrh) separated into the different loading states (loaded with BC and ammonium sulfate) and minimum and maximum loading areal density on the filter. Dashed and colored lines represent the linear regression fit. Red and blue colors indicate MA200 at 625 nm and black and green colors indicate STAP at 624 nm. In the first panel BC loading is shown whereas in the second panel the ammonium sulfate case is displayed. Coefficients of the linear regression fit are displayed in panel 3. Shading of color in the linear fits and of the points are same as in panel 3.

675

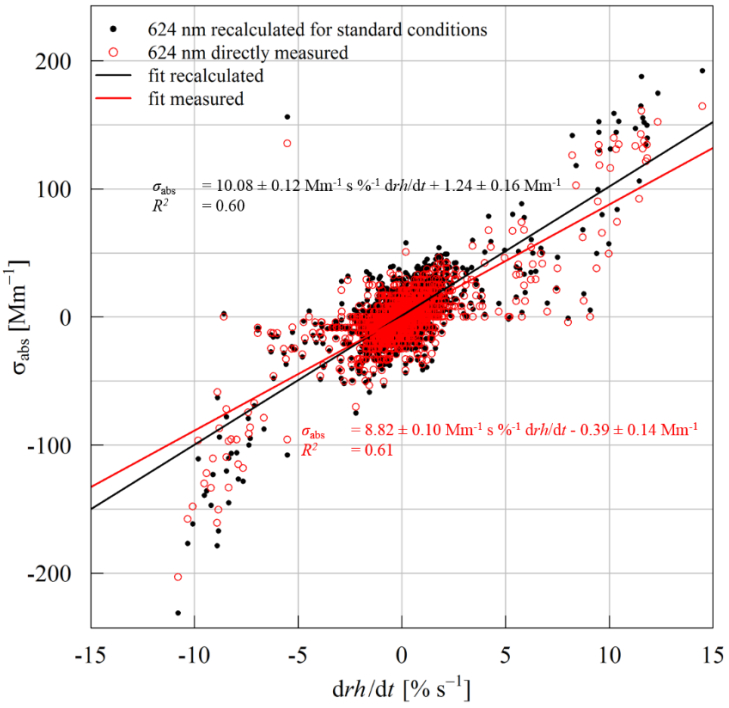

Figure 8: Scatterplot of σ_{abs} and change rate of *rh* (d*rh*/d*t*) at 624 nm derived directly from STAP without any corrections (red) and recalculated σ_{abs} at 624 nm including corrections to standard conditions (black). Linear fit equations and correlation coefficient are given in the corresponding colors.

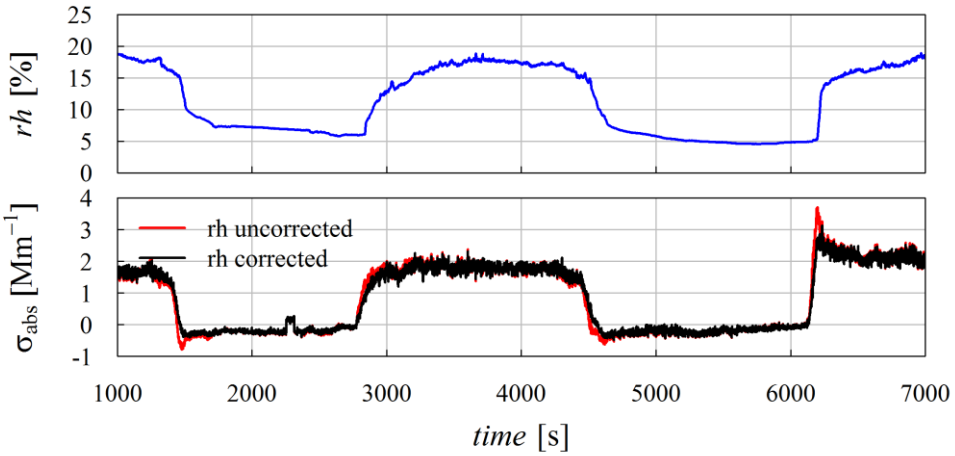

Figure 9: Time series of *rh* before the inlet of the STAP (blue, upper panel) and recalculated σ_{abs} (running 60 s mean of 1 Hz calculations) at standard conditions corrected (black) and uncorrected (red) for *rh* changes.

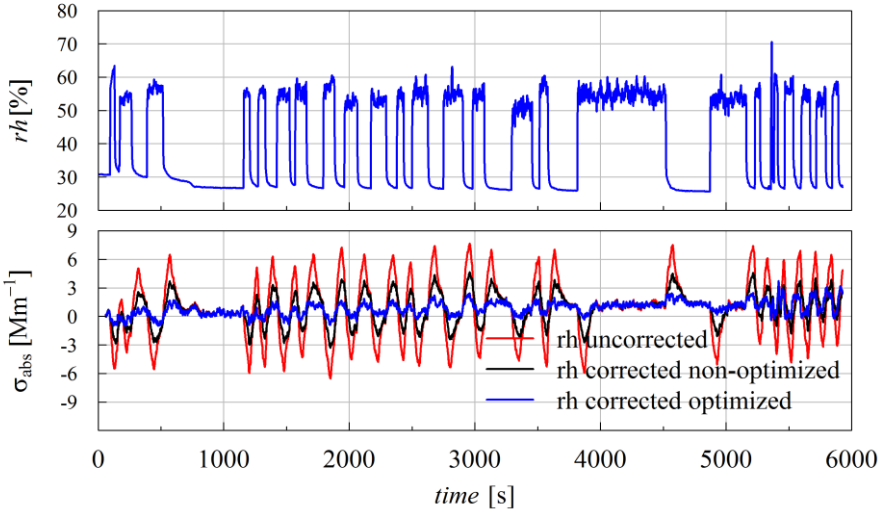

Figure 10: Time series of a laboratory measurement of σ_{abs} conducted with the MA200 without a filter. Upper panel shows the *rh* of the aerosol sample and the lower panel displays the 60 s running average of measured σ_{abs} at 1 Hz time resolution and 625 nm uncorrected and biased by *rh* changes (red) and corrected with the modelled σ_{abs} derived with the ARMA-X model (black).

680